p.[L461V;V716_R730del], p.I619del, p.R666W and p.V716_R730del were completely defective in NER of UV-induced DNA damage. Additionally, although p.L461V and p.A717G possessed full NER activity (comparable to p.WT), the combined mutant p.[L461V;A717G] possessed only partial NER activity.

TFIIH-forming activity of mutated XPDs

The results of the UV survival assays shown in Figures 3a and b prompted us to investigate the ability of the XPD variants to form the TFIIH complex. To this end, we subjected whole-cell extracts from XP6BESV cells expressing various XPD proteins to immunoprecipitation with anti-FLAG antibodies. p.G47R, p.R666W and p.A717G could bind components of TFIIH, including XPG, as efficiently as p.WT (Figure 3c, lanes 2–4 and 10), whereas p.I619del, p.V716_R730del and p.[L461V;V716_R730del] could not (Figure 3c, lanes 5, 6 and 9). Additionally, p.L461V and p.[L461V;A717G] co-immunoprecipitated with components of TFIIH, including XPG, but only weakly (Figure 3c, lanes 7 and 8). These results indicated that p.G47R, p.R666W and p.A717G could form TFIIH complex normally, whereas p.I619del, p.V716_R730del and p.[L461V;V716_R730del] could not. Additionally, p.L461V and p.[L461V;A717G] formed the TFIIH complex to some extent, but they could not do so as efficiently as the WT protein.

DISCUSSION

We describe here two Japanese patients who exhibited COFS symptoms caused by mutations in the *XPD* gene. *XPD* gene mutations give rise to XP and XP/CS in addition to COFS. On the basis of *XPD* genotype–phenotype relationships, different clinical symptoms were strongly associated with various mutations in the *XPD* gene.

COFS-Chiba1 and COFS-05-135, described in this report, and XP-D/CS patients XP1JI and XPCS1PV, described previously,[19,20,23] had very severe symptoms and died at ages of 5 months to 2 years (Table 1). COFS represents the most severe end of the CS spectrum;[8] therefore, we refer to these cases here as severe-XP-D/CS. p.I619Del, found in the two COFS patients described here, did not bind to the core complex of TFIIH (Figure 3c, lane 6) and could not rescue the NER defect of XP1BESV cell lines (Figure 3b). From these findings, we conclude that p.I619del is functionally null, and that only p.G47R or p.R666W was expressed as functional XPD in these COFS patients; single expression of p.G47R and p.R666W was the cause of severe XP-D/CS in XP1JI and XPCS1PV, respectively.[19,20] Both p.G47R and p.R666W could bind and form TFIIH complex components, including XPG (Figure 3c, lanes 3 and 4), but neither protein could rescue the NER defect of XP6BESV cell lines (Figure 3a), indicating that both p.G47R and p.R666W completely lack NER activity. Previous biochemical examination revealed that p.G47R is defective in ATPase, helicase, DNA repair synthesis and dual-incision activities.[24] There is no detailed biochemical information regarding human p.R666W, but structural and biochemical analyses have been performed on the *Sulfolobus acidocaldarius* XPD homolog.[25] The *Sulfolobus acidocaldarius* XPD mutants p.G34R and p.R514W, which, respectively, correspond to human XPD p.G47R and p.R666W, are defective in ATPase and helicase activities. These biochemical results indicate that p.G47R and p.R666W have lost the ability to engage in basal transcription; nevertheless, both mutants can still form TFIIH complex (Figure 3c, lanes 3 and 4). Based on these observations, we conclude that sole expression of p.G47R or p.R666W caused the severe manifestations found in these patients.

On the other hand, XP1NE and XPCS118LV exhibited typical XP features along with neurological disease, and both patients survived beyond 30 years of age: XP1NE and XPCS118LV died at 43 and 37 years, respectively.[19,20,23] Here we refer to these milder symptoms as mild XP-D/CS. A previous report indicated that p.[G47R];[L461V;V716_R730del] and p.[L461V;V716_R730del];[R666W] are the causes of XP1NE and XPCS118LV, respectively.[20,21] However, we observed that authentic splicing resulted in the p.A717G amino-acid change, and that consequently, p.[L461V;A717G] was expressed from the p.[L461V;V716_R730del]-encoding allele (Figure 2). Therefore, it is clear that three kinds of mutated XPD protein are expressed in XP1NE (p.[G47R];[L461V;A717G,V716_R730del]) and XPCS118LV (p.[L461V;A717G,V716_R730del];[R666W]), as shown in Table 1. The p.[L461V;V716_R730del] mutation cannot rescue lethality in a *rad15* mutant of *Schizosaccharomyces pombe*.[21] Furthermore, biochemical analysis revealed that the single p.V716_R730del mutant protein lacks the ability to bind to p44 (ref. 22) and has a defect in basal transcription.[24] Additionally, p.L461V has NER activity comparable to that of p.WT, although the p.L461V mutant forms a loose conformation of TFIIH (Figures 3b and c). These observations indicate that p.[L461V;V716_R730del] is functionally null because of the p.V716_R730del mutation. p.A717G formed TFIIH as competently as p.WT (Figure 3c, lane 10) and rescued the UV hypersensitivity of XP6BESV as well as p.WT (Figure 3b), indicating that p.A717G might possess full XPD function. In the case of compound-mutated XPD, that is, p.[L461V;A717G], the ability to bind core TFIIH was reduced, as in the case of p.L461V (Figure 3c, lane 10), suggesting that the p.L461V mutation affected the binding ability of p.A717G. Interestingly, p.[L461V;A717G] had partial NER activity (Figure 3b). These observations suggest that the low TFIIH-binding capacity of p.[L461V;A717G] might affect basal transcription and cause the mild XP-D/CS clinical features, although the basal transcription ability of p.[L461V;A717G] remains unknown.

The p.[L461V;V716_R730del]-encoding allele has been considered to be functionally null.[20,21,23] However, we conclude that coexpression of p.[L461V;A717G] because of authentic splicing in the mild XP-D/CS patients partially rescues the functional defect of p.G47R or p.R666W, resulting in a more than 10-fold increase in lifespan in mild XP-D/CS patients relative to patients with severe XP-D/CS.

CONFLICT OF INTEREST

The authors declare no conflict of interest.

ACKNOWLEDGEMENTS

This work was supported by a Grant-in-Aid for Scientific Research from the Ministry of Education, Culture, Sports, Science, and Technology (MEXT) of Japan.

1 Pena, S. D. & Shokeir, M. H. Autosomal recessive cerebro-oculo-facio-skeletal (COFS) syndrome. *Clin. Genet.* **5**, 285–293 (1974).
2 Graham, J. M. Jr, Anyane-Yeboa, K., Raams, A., Appeldoorn, E., Kleijer, W. J. & Garritsen, V. H. *et al.* Cerebro-oculo-facio-skeletal syndrome with a nucleotide excision-repair defect and a mutated XPD gene, with prenatal diagnosis in a triplet pregnancy. *Am. J. Hum. Genet.* **69**, 291–300 (2001).
3 Frederick, G. D., Amirkhan, R. H., Schultz, R. A. & Friedberg, E. C. Structural and mutational analysis of the xeroderma pigmentosum group D (XPD) gene. *Hum. Mol. Genet.* **3**, 1783–1788 (1994).
4 Takayama, K., Salazar, E. P., Lehmann, A., Stefanini, M., Thompson, L. H. & Weber, C. A. Defects in the DNA repair and transcription gene ERCC2 in the cancer-prone disorder xeroderma pigmentosum group D. *Cancer Res.* **55**, 5656–5663 (1995).
5 Broughton, B. C., Thompson, A. F., Harcourt, S. A., Vermeulen, W., Hoeijmakers, J. H. & Botta, E. *et al.* Molecular and cellular analysis of the DNA repair defect in a patient in xeroderma pigmentosum complementation group D who has the clinical features of

xeroderma pigmentosum and Cockayne syndrome. *Am. J. Hum. Genet.* **56**, 167–174 (1995).
6 Nance, M. A. & Berry, S. A. Cockayne syndrome: review of 140 cases. *Am. J. Med. Genet.* **42**, 68–84 (1992).
7 Graham, J. M. Jr., Hennekam, R., Dobyns, W. B., Roeder, E. & Busch, D. MICRO syndrome: an entity distinct from COFS syndrome. *Am. J. Med. Genet. Part A* **128A**, 235–245 (2004).
8 Laugel, V., Dalloz, C., Tobias, E. S., Tolmie, J. L., Martin-Coignard, D. & Drouin-Garraud, V. *et al.* Cerebro-oculo-facio-skeletal syndrome: three additional cases with CSB mutations, new diagnostic criteria and an approach to investigation. *J. Med. Genet.* **45**, 564–571 (2008).
9 Hanawalt, P. C. & Spivak, G. Transcription-coupled DNA repair: two decades of progress and surprises. *Nature reviews. Nat. Rev. Mol. Cell Biol.* **9**, 958–970 (2008).
10 Drapkin, R., Reardon, J. T., Ansari, A., Huang, J. C., Zawel, L. & Ahn, K. *et al.* Dual role of TFIIH in DNA excision repair and in transcription by RNA polymerase II. *Nature* **368**, 769–772 (1994).
11 Schaeffer, L., Moncollin, V., Roy, R., Staub, A., Mezzina, M. & Sarasin, A. *et al.* The ERCC2/DNA repair protein is associated with the class II BTF2/TFIIH transcription factor. *EMBO J.* **13**, 2388–2392 (1994).
12 Egly, J. M. & Coin, F. A history of TFIIH: two decades of molecular biology on a pivotal transcription/repair factor. *DNA Repair (Amst)* **10**, 714–721 (2011).
13 Cleaver, J. E., Lam, E. T. & Revet, I. Disorders of nucleotide excision repair: the genetic and molecular basis of heterogeneity. *Nat. Rev. Genet.* **10**, 756–768 (2009).
14 Hashimoto, S. & Egly, J. M. Trichothiodystrophy view from the molecular basis of DNA repair/transcription factor TFIIH. *Hum. Mol. Genet.* **18**, R224–R230 (2009).
15 Stefanini, M., Botta, E., Lanzafame, M. & Orioli, D. Trichothiodystrophy: from basic mechanisms to clinical implications. *DNA Repair (Amst)* **9**, 2–10 (2010).
16 Fuss, J. O. & Tainer, J. A. XPB and XPD helicases in TFIIH orchestrate DNA duplex opening and damage verification to coordinate repair with transcription and cell cycle via CAK kinase. *DNA Repair (Amst)* **10**, 697–713 (2011).
17 DiGiovanna, J. J. & Kraemer, K. H. Shining a light on xeroderma pigmentosum. *J. Invest. Dermatol.* **132**, 785–796 (2012).
18 Kobayashi, T., Kuraoka, I., Saijo, M., Nakatsu, Y., Tanaka, A. & Someda, Y. *et al.* Mutations in the XPD gene leading to xeroderma pigmentosum symptoms. *Hum. Mut.* **9**, 322–331 (1997).
19 Fujimoto, M., Leech, S. N., Theron, T., Mori, M., Fawcett, H. & Botta, E. *et al.* Two new XPD patients compound heterozygous for the same mutation demonstrate diverse clinical features. *J. Invest. Dermatol.* **125**, 86–92 (2005).
20 Theron, T., Fousteri, M. I., Volker, M., Harries, L. W., Botta, E. & Stefanini, M. *et al.* Transcription-associated breaks in xeroderma pigmentosum group D cells from patients with combined features of xeroderma pigmentosum and Cockayne syndrome. *Mol. Cell. Biol.* **25**, 8368–8378 (2005).
21 Taylor, E. M., Broughton, B. C., Botta, E., Stefanini, M., Sarasin, A. & Jaspers, N. G. *et al.* Xeroderma pigmentosum and trichothiodystrophy are associated with different mutations in the XPD (ERCC2) repair/transcription gene. *Proc. Natl Acad. Sci. USA* **94**, 8658–8663 (1997).
22 Coin, F., Marinoni, J. C., Rodolfo, C., Fribourg, S., Pedrini, A. M.. & Egly, J. M. Mutations in the XPD helicase gene result in XP and TTD phenotypes, preventing interaction between XPD and the p44 subunit of TFIIH. *Nat. Genet.* **20**, 184–188 (1998).
23 Andressoo, J. O., Jans, J., de Wit, J., Coin, F., Hoogstraten, D. & van de Ven, M. *et al.* Rescue of progeria in trichothiodystrophy by homozygous lethal Xpd alleles. *PLoS Biol.* **4**, e322 (2006).
24 Dubaele, S., Proietti De Santis, L., Bienstock, R. J., Keriel, A., Stefanini, M. & Van Houten, B. *et al.* Basal transcription defect discriminates between xeroderma pigmentosum and trichothiodystrophy in XPD patients. *Mol. Cell* **11**, 1635–1646 (2003).
25 Fan, L., Fuss, J. O., Cheng, Q. J., Arvai, A. S., Hammel, M. & Roberts, V. A. *et al.* XPD helicase structures and activities: insights into the cancer and aging phenotypes from XPD mutations. *Cell* **133**, 789–800 (2008).

Supplementary Information accompanies the paper on Journal of Human Genetics website (http://www.nature.com/jhg)

Genes and Environment, Vol. 36, No. 4 pp. 199–202 (2014)

Short communication

Evaluation of Rats' *In Vivo* Genotoxicity Induced by *N*-ethyl-*N*-nitrosourea in the RBC *Pig-a*, PIGRET, and *gpt* Assays

Katsuyoshi Horibata[1], Akiko Ukai and Masamitsu Honma

Division of Genetics and Mutagenesis, National Institute of Health Sciences, Tokyo, Japan

Received June 23, 2014; Revised August 14, 2014; Accepted August 25, 2014
J-STAGE Advance published date: August 30, 2014

The emerging *Pig-a* gene mutation assay, a powerful and promising tool for evaluating *in vivo* genotoxicity, is based on flow cytometric enumeration of red blood cells (RBCs), which are deficient in glycosylphosphatidylinositol anchored protein. Various approaches for measuring *Pig-a* mutant cells have been developed, particularly those focused on peripheral RBCs and reticulocytes (RETs). Previously, it had been reported that *Pig-a* and *gpt* mutant frequencies were relatively increased in *N*-ethyl-*N*-nitrosourea (ENU)- and benzo[*a*]pyrene (BP)-treated mice. The capacity and characteristics of the *Pig-a* assay relative to transgenic rodent (TGR) mutation assays, however, are unclear in rats. Here, using transgenic *gpt* delta rats, we compared the *in vivo* genotoxicity of single oral doses of ENU (40 mg/kg) in the *gpt* gene mutation assay in bone marrow and liver, and *Pig-a* gene mutation assays on RBCs and RETs in the same animals. The *Pig-a* gene mutation assays were conducted at 1, 2, and 4 weeks after treatment, whereas *gpt* assays were conducted on tissues collected at the 4-week terminal sacrifice. Consequently, we detected that *Pig-a* and *gpt* mutant frequencies were clearly increased in ENU-treated rats, indicating that both the *Pig-a* and TGR gene mutation assays can detect *in vivo* ENU genotoxicity equally.

Key words: transgenic rodent mutation assays; glycosylphosphatidylinositol anchor; red blood cells; reticulocyte

Introduction

Because gene mutations are implicated in the etiology of cancer and other human diseases, *in vivo* genotoxicity tests are important as public health management tools. One such tool is the transgenic rodent (TGR) mutation assay, which permits quantitative and accumulative evaluation of genotoxicity in all organs (1). The TGR mutation assay fulfills a need for a practical and widely available *in vivo* test for assessing gene mutation, and this assay has been recommended by regulatory authorities for safety evaluations (2,3) and international guidelines have been published describing the conduct of the assay (4).

The emerging *Pig-a* gene mutation assay, a powerful and promising tool for the evaluation of *in vivo* genotoxicity, was recently developed (5–7). Because the *Pig-a* gene is X-chromosome linked and involves the first step of glycosylphosphatidylinositol (GPI) anchor biosynthesis, the forward mutation can result in the loss of GPI-anchored protein expression (7). Additionally, *Pig-a* mutation appears to function in a neutral manner whereby the accumulated effects of repeat exposures can be evaluated.

Various approaches for measuring *Pig-a* mutant cells have specifically focused on peripheral red blood cells (RBCs) and reticulocytes (RETs) (8–18). In these reports, although SYTO 13 dye or an antibody against the rat erythroid marker, HIS49, was used to label RETs in whole bloods, there was a limited capacity for counting RETs by flow cytometer. Conversely, a recently developed assay for measuring *Pig-a* mutant RETs, that is the PIGRET assay, is capable of flow cytometric cell counting $>1\times10^6$ RETs for the *Pig-a* mutant by concentrating RETs in whole bloods (19) and the approaches can be technically transferred between laboratories (20).

In this study, we performed the *gpt* and *Pig-a* gene mutation assays on RBCs (RBC *Pig-a* assay) and RETs (PIGRET assay) in the same animals, and we compared their performance in detecting ENU genotoxicity. This report describes the performance, effectiveness, and advantages of the RBC *Pig-a* and PIGRET assays in comparison with the *gpt* assay.

Materials and Methods

Preparation of chemicals: We dissolved ENU (Sigma-Aldrich Japan, Tokyo) in phosphate-buffered saline (PBS; pH 6.0) at 10 mg/mL.

Antibodies: We obtained anti-rat CD59 (clone

[1]Correspondence to: Katsuyoshi Horibata, Division of Genetics and Mutagenesis, National Institute of Health Sciences, 1-18-1 Kamiyoga, Setagaya-ku, Tokyo 158-8501, Japan. Tel: +81-3-3700-1141, Fax: +81-3-3700-2348, E-mail: horibata@nihs.go.jp
doi: org/10.3123/jemsge.2014.023

TH9, FITC-conjugated), anti-rat CD71 (clone OX-26, PE-conjugated), and anti-rat erythroid marker (clone HIS49, APC-conjugated) antibodies from BD Biosciences (Tokyo, Japan).

Treatment of rats: Animal experiments were conducted humanely according to the regulations of the Animal Care and Use Committee of the National Institute of Health Sciences, Tokyo, and with their permission. *gpt* delta Wistar Hannover transgenic male rats were obtained from Japan SLC (Shizuoka, Japan). They were housed individually under specific pathogen-free conditions with a 12-h light-dark cycle and given tap water and autoclaved CRF-1 pellets (Oriental Yeast Co., Ltd., Tokyo) *ad libitum*. At 8 weeks of age, 5 rats per group were given a single oral administration of ENU (40 mg/kg) or PBS (negative control). Peripheral blood (120 μL) was withdrawn from a tail vein 1, 2, and 4 weeks after the treatments and used for the RBC *Pig-a* and PIGRET assays. At 4 weeks, all rats were sacrificed and the bone marrow and liver samples were collected for the *gpt* assay.

***Pig-a* mutation assays:** The RBC *Pig-a* and PIGRET assays were performed as previously described (5,19,20). Peripheral blood was withdrawn and immediately transferred into EDTA (dipotassium salt)-coated Microtainer® Tubes (BD Biosciences). For the RBC *Pig-a* assay, 3 μL of blood was suspended in 0.2 mL PBS and labeled with anti-rat CD59 (1 μg) and anti-rat erythroid marker (0.133 μg) antibodies. The cells were incubated for 1 h in the dark at room temperature, centrifuged (1,680 × g, 5 min), resuspended in 1 mL PBS, and examined using a FACS Canto II flow cytometer (BD Biosciences). After gating for single cells, approximately 1×10^6 erythroid marker-positive cells were analyzed for the presence of surface CD59 and the *Pig-a* mutant frequency (MF) was calculated as previously described (19,20). For the PIGRET assay, 80 μL of blood was suspended in 0.2 mL PBS and labeled with 1 μg of PE-conjugated anti-rat CD71 antibody. The cells were incubated for 15 min in the dark on ice. After washing with 2 mL of 1 × IMag Buffer (BD Biosciences) and centrifuged (1680 × g, 5 min), the cells were mixed with 50 μL of BD IMag PE Particles Plus-DM (BD Biosciences) and incubated for 15 min in a refrigerator (4°C). The samples were enriched for CD71-positive cells by processing with a BD IMagnet magnetic stand (BD Biosciences) according to the manufacturer's instructions. The enriched samples were labeled with HIS49 and anti-CD59 antibodies as indicated for total RBC labeling, with the exception that the incubation time for labeling enriched RETs was half that for the total RBCs. The final cell suspension volume was 500 μL. *Pig-a* MF of CD71-positive RETs was examined using a FACS Canto II flow cytometer (BD Biosciences) as previously described (19,20).

***gpt* mutation assay:** We extracted high molecular weight genomic DNA from the liver and bone marrow samples using a Recover Ease DNA Isolation Kit (Agilent Technologies, Santa Clara, CA, USA), rescued lambda EG10 phages using Transpack Packaging Extract (Agilent Technologies), and conducted the *gpt* mutation assay as previously described (1). *gpt* Mutant frequencies (MFs) were calculated by dividing the number of confirmed 6-thioguanine-resistant colonies by the number of colonies with rescued plasmids (1).

Statistical Analyses: The Mann-Whitney U-test was used for comparisons between PBS- and ENU-treated groups at each time point. Statistical analyses were performed using Prism 6 for Mac OS X (GraphPad Software, Inc., La Jolla, CA, USA). For these analyses, a p-value of <0.05 was considered significant and one-tailed tests were performed.

Results

The *Pig-a* assay: *Pig-a* MFs of whole RBCs (RBC *Pig-a* MF) in the ENU-treated rats were significantly increased, and the increase was modestly time-dependent (mean ± SD for rats treated with PBS: pre-treatment, $3.20 \pm 1.79 \times 10^{-6}$; 1 week after treatment, $1.80 \pm 1.30 \times 10^{-6}$; 2 weeks after treatment, $0.80 \pm 0.45 \times 10^{-6}$; and 4 weeks after treatment, $2.20 \pm 2.28 \times 10^{-6}$; mean ± SD for rats treated with 40 mg/kg ENU: pre-treatment, $2.80 \pm 2.28 \times 10^{-6}$; 1 week after treatment, $4.60 \pm 1.67 \times 10^{-6}$; 2 weeks after treatment, $31.4 \pm 5.86 \times 10^{-6}$; and 4 weeks after treatment, $52.80 \pm 8.84 \times 10^{-6}$) (Fig. 1A).

In the case of *Pig-a* MFs of RETs (RET *Pig-a* MF), significant increases were detected 1 week after treatment (mean ± SD for rats treated with PBS: pre-treatment, $3.00 \pm 4.81 \times 10^{-6}$; 1 week after treatment, $1.80 \pm 1.92 \times 10^{-6}$; 2 weeks after treatment, $2.80 \pm 1.64 \times 10^{-6}$; and 4 weeks after treatment, $0.80 \pm 0.84 \times 10^{-6}$; mean ± SD for rats treated with 40 mg/kg ENU: pre-treatment, $3.60 \pm 3.21 \times 10^{-6}$; 1 week after treatment, $107.6 \pm 10.5 \times 10^{-6}$; 2 weeks after treatment, $126.6 \pm 15.6 \times 10^{-6}$; and 4 weeks after treatment, $162.6 \pm 54.89 \times 10^{-6}$) (Fig. 1B).

The *gpt* assay on the bone marrow and liver samples

Compared with the solvent control animals (MF for PBS control group, $17.05 \pm 12.10 \times 10^{-6}$), significant increases in bone marrow *gpt* MFs were observed in ENU-treated rats [$87.39 \pm 60.55 \times 10^{-6}$ (Fig. 2)]. *gpt* MFs were also increased in the liver samples (MF for PBS control group, $7.56 \pm 7.97 \times 10^{-6}$; ENU, $79.04 \pm 31.62 \times 10^{-6}$) (Fig. 2).

Discussion

Here, we showed ENU genotoxicity using three different methods: the RBC *Pig-a*, PIGRET, and TGR

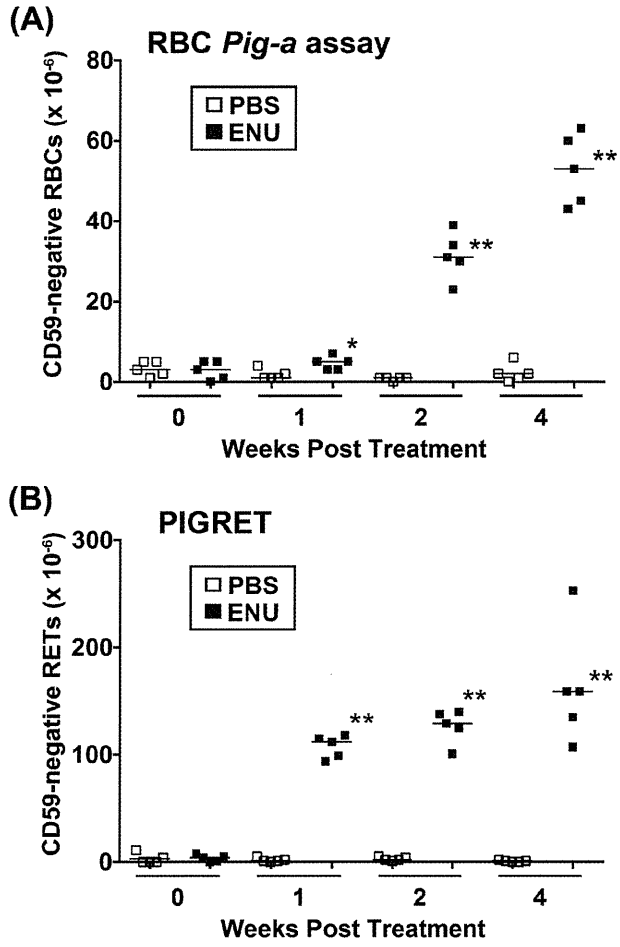

Fig. 1. Comparative analyses of the RBC *Pig-a* (A) and PIGRET (B) assays. At 1, 2, and 4 weeks after treatment with 40 mg/kg ENU or PBS solvent, peripheral blood was withdrawn from the tail vein and analyzed by flow cytometry for the presence of surface CD59 on RBCs or RETs. $^{*}p<0.05$, $^{**}p<0.01$.

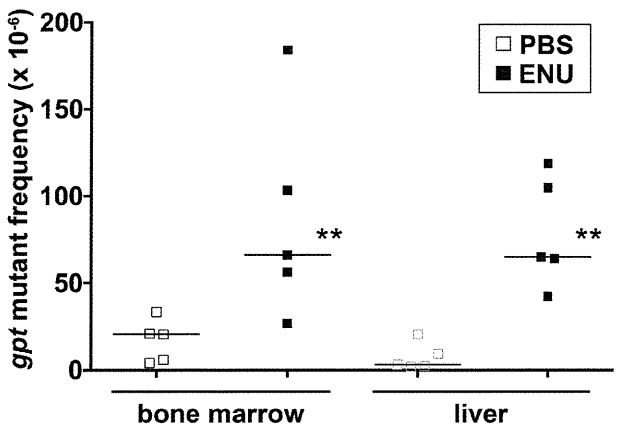

Fig. 2. *gpt* Mutation frequencies in the bone marrow and liver samples. Four weeks after treatment, all rats were sacrificed and their bone marrow and liver samples were collected and analyzed by the *gpt* assay. $^{**}p<0.01$.

mutation assays in rats. Although TGR mutation assays, such as the *gpt* gene mutation assay performed here, are well established methods and permit the *in vivo* evaluation of genotoxicity in more than one organ concurrently (1,4,21), they are costly and need TGR animals. While the *Pig-a* gene mutation assays, including the PIGRET assay, analyze only one type of cells (i.e., blood cells), these assays have the advantage of not using transgenic animals (5,6) and strong potential to be integrated into repeat-dose toxicology studies because accumulated effects can be evaluated (8–10). Additionally, compared with the RBC *Pig-a* assay, the PIGRET assay can detect increases in *Pig-a* MF sooner after exposure (20).

The results of our RBC *Pig-a* and PIGRET assays indicated that the latter more consistently detected ENU-induced increases in *Pig-a* MF at early sampling times than the former (Fig. 1). These results obtained using a single oral administration of ENU were consistent with those previously reported (15,19,20). The ENU-induced *gpt* MFs on the bone marrow and liver samples were well detected as MFs of the RBC *Pig-a* and PIGRET assays (Fig. 2), suggesting that both assays were equally able to detect ENU genotoxicity.

The OECD guideline for TGR assays recommends a tissue sampling time of 3 days after 28 consecutive daily treatments (4), making it difficult to integrate TGR assays into standard repeat-dose toxicology studies. Because the *Pig-a* gene is an endogenous gene, the *Pig-a* assay can be combined with a TGR assay as was done in this present and a previous study (14), and it also can potentially be integrated into repeat-dose toxicology studies that do not use TGRs (8,9,11,12,16,17,22–24). Additionally, the PIGRET assay has strong potential to detect genotoxicity in an early stage of the study, e.g., at 1 week after exposure. Currently, however, we need additional studies that compare mutational responses in the *Pig-a* gene and TGR transgenes to help validate the *Pig-a* assays.

Acknowledgments: This work was supported by Health and Labor Sciences Research Grant Number H24-chemical-appointed-009 and H25-chemical-young-008, Japan, and Health Science Foundation Grant Number KHB1209, Japan. We would like to thank Dr. Kaoru Inoue for the technical advice.

Disclosure statement: The authors declare no conflict of interest.

References

1 Nohmi T, Suzuki T, Masumura K. Recent advances in the protocols of transgenic mouse mutation assays. Mutat Res. 2000; 455: 191–215.

2 COM. Guidance on a strategy for genotoxicity testing of

chemical substances.: Committee on Mutagenicity of Chemicals in Food, Consumers Products, and the Environment (COM). 2011.
3 ICH. The ICH S2(R1) Guideline on Genotoxicity Testing and Data Interpretation for Pharmaceuticals Intended for Human Use. Guidance on Genotoxicity Testing and Data Interpretation for Pharmaceuticals Intended for Human Use: The International Conference on Harmonisation of Technical Requirements for Registration of Pharmaceuticals for Human Use. 2011.
4 OECD 488. Test guideline 488: OECD guideline for the testing of chemicals. Transgenic Rodent Somatic and Germ Cell Gene Mutation Assays. Paris: Organisation for Economic Cooperation and Development. 2011.
5 Miura D, Dobrovolsky VN, Kasahara Y, Katsuura Y, Heflich RH. Development of an in vivo gene mutation assay using the endogenous Pig-A gene: I. Flow cytometric detection of CD59-negative peripheral red blood cells and CD48-negative spleen T-cells from the rat. Environ Mol Mutagen. 2008; 49: 614–21.
6 Miura D, Dobrovolsky VN, Mittelstaedt RA, Kasahara Y, Katsuura Y, Heflich RH. Development of an in vivo gene mutation assay using the endogenous Pig-A gene: II. Selection of Pig-A mutant rat spleen T-cells with proaerolysin and sequencing Pig-A cDNA from the mutants. Environ Mol Mutagen. 2008; 49: 622–30.
7 Miura D, Dobrovolsky VN, Kimoto T, Kasahara Y, Heflich RH. Accumulation and persistence of Pig-A mutant peripheral red blood cells following treatment of rats with single and split doses of N-ethyl-N-nitrosourea. Mutat Res. 2009; 677: 86–92.
8 Dertinger SD, Phonethepswath S, Franklin D, Weller P, Torous DK, Bryce SM, et al. Integration of mutation and chromosomal damage endpoints into 28-day repeat dose toxicology studies. Toxicol Sci. 2010; 115: 401–11.
9 Shi J, Krsmanovic L, Bruce S, Kelly T, Paranjpe M, Szabo K, et al. Assessment of genotoxicity induced by 7,12-dimethylbenz(a)anthracene or diethylnitrosamine in the Pig-a, micronucleus and Comet assays integrated into 28-day repeat dose studies. Environ Mol Mutagen. 2011; 52: 711–20.
10 Stankowski LF, Roberts DJ, Chen H, Lawlor T, McKeon M, Murli H, et al. Integration of Pig-a, micronucleus, chromosome aberration, and comet assay endpoints in a 28-day rodent toxicity study with 4-nitroquinoline-1-oxide. Environ Mol Mutagen. 2011; 52: 738–47.
11 Lynch AM, Giddings A, Custer L, Gleason C, Henwood A, Aylott M, et al. International Pig-a gene mutation assay trial (Stage III): Results with N-methyl-N-nitrosourea. Environmental and Molecular Mutagenesis. 2011; 52: 699–710.
12 Dertinger SD, Phonethepswath S, Weller P, Avlasevich S, Torous DK, Mereness JA, et al. Interlaboratory Pig-a gene mutation assay trial: Studies of 1,3-propane sultone with immunomagnetic enrichment of mutant erythrocytes. Environ Mol Mutagen. 2011; 52: 748–55.
13 Dobrovolsky VN, Boctor SY, Twaddle NC, Doerge DR, Bishop ME, Manjanatha MG, et al. Flow cytometric detection of Pig-A mutant red blood cells using an erythroid-specific antibody: application of the method for evaluating the in vivo genotoxicity of methylphenidate in adolescent rats. Environ Mol Mutagen. 2010; 51: 138–45.
14 Horibata K, Ukai A, Kimoto T, Suzuki T, Kamoshita N, Masumura K, et al. Evaluation of in vivo genotoxicity induced by N-ethyl-N-nitrosourea, benzo[a]pyrene, and 4-nitroquinoline-1-oxide in the Pig-a and gpt assays. Environ Mol Mutagen. 2013; 54: 747–54.
15 Horibata K, Ukai A, Koyama N, Takagi A, Kanno J, Kimoto T, et al. Fullerene (C60) is negative in the in vivo Pig-A gene mutation assay. Genes Environ. 2011; 33: 27–31.
16 Cammerer Z, Bhalli JA, Cao X, Coffing SL, Dickinson D, Dobo KL, et al. Report on stage III Pig-a mutation assays using N-ethyl-N-nitrosourea–comparison with other in vivo genotoxicity endpoints. Environ Mol Mutagen. 2011; 52: 721–30.
17 Bhalli JA, Shaddock JG, Pearce MG, Dobrovolsky VN, Cao X, Heflich RH, et al. Report on stage III Pig-a mutation assays using benzo[a]pyrene. Environ Mol Mutagen. 2011; 52: 731–7.
18 Phonethepswath S, Franklin D, Torous DK, Bryce SM, Bemis JC, Raja S, et al. Pig-a mutation: kinetics in rat erythrocytes following exposure to five prototypical mutagens. Toxicol Sci. 2010; 114: 59–70.
19 Kimoto T, Chikura S, Suzuki K, Kobayashi Xm, Itano Y, Horibata K, et al. Further development of the rat Pig-a mutation assay: Measuring rat Pig-a mutant bone marrow erythroids and a high throughput assay for mutant peripheral blood reticulocytes. Environ Mol Mutagen. 2011; 52: 774–83.
20 Kimoto T, Horibata K, Chikura S, Hashimoto K, Itoh S, Sanada H, et al. Interlaboratory trial of the rat Pig-a mutation assay using an erythroid marker HIS49 antibody. Mutat Res. 2013; 755: 126–34.
21 Lambert IB, Singer TM, Boucher SE, Douglas GR. Detailed review of transgenic rodent mutation assays. Mutat Res. 2005; 590: 1–280.
22 Dobrovolsky VN, Miura D, Heflich RH, Dertinger SD. The in vivo Pig-a gene mutation assay, a potential tool for regulatory safety assessment. Environ Mol Mutagen. 2010; 51: 825–35.
23 Lemieux CL, Douglas GR, Gingerich J, Phonethepswath S, Torous DK, Dertinger SD, et al. Simultaneous measurement of benzo[a]pyrene-induced Pig-a and lacZ mutations, micronuclei and dna adducts in mutaTMmouse. Environ Mol Mutagen. 2011; 52: 756–65.
24 Schuler M, Gollapudi BB, Thybaud V, Kim JH. Need and potential value of the Pig-a in vivo mutation assay-A hesi perspective. Environmental and Molecular Mutagenesis. 2011; 52: 685–9.

THE JOURNAL OF BIOLOGICAL CHEMISTRY VOL. 289, NO. 41, pp. 28730–28737, October 10, 2014

Nucleotide Excision Repair-dependent DNA Double-strand Break Formation and ATM Signaling Activation in Mammalian Quiescent Cells*

Received for publication, July 4, 2014, and in revised form, August 25, 2014 Published, JBC Papers in Press, August 27, 2014, DOI 10.1074/jbc.M114.589747

Mitsuo Wakasugi[‡1], **Takuma Sasaki**[‡1], **Megumi Matsumoto**[‡], **Miyuki Nagaoka**[‡], **Keiko Inoue**[‡], **Manabu Inobe**[‡], **Katsuyoshi Horibata**[§2], **Kiyoji Tanaka**[§], **and Tsukasa Matsunaga**[‡3]

From the [‡]*Faculty of Pharmacy, Institute of Medical, Pharmaceutical and Health Sciences, Kanazawa University, Kakuma-machi, Kanazawa 920-1192, Japan and the* [§]*Human Cell Biology Group, Graduate School of Frontier Biosciences, Osaka University, 1-3 Yamadaoka, Suita, Osaka 565-0871, Japan*

Background: In quiescent human cells, UV induces histone H2AX phosphorylation by ATR in a nucleotide excision repair (NER)-dependent manner.
Results: UV also activates ATM in response to NER-mediated DNA double-strand break (DSB).
Conclusion: The NER reaction in quiescent cells potentially generates multiple types of secondary DNA damage.
Significance: This work highlights the importance of our understanding of the DNA damage response in quiescent cells.

Histone H2A variant H2AX is phosphorylated at Ser^{139} in response to DNA double-strand break (DSB) and single-stranded DNA (ssDNA) formation. UV light dominantly induces pyrimidine photodimers, which are removed from the mammalian genome by nucleotide excision repair (NER). We previously reported that in quiescent G_0 phase cells, UV induces ATR-mediated H2AX phosphorylation plausibly caused by persistent ssDNA gap intermediates during NER. In this study, we have found that DSB is also generated following UV irradiation in an NER-dependent manner and contributes to an earlier fraction of UV-induced H2AX phosphorylation. The NER-dependent DSB formation activates ATM kinase and triggers the accumulation of its downstream factors, MRE11, NBS1, and MDC1, at UV-damaged sites. Importantly, ATM-deficient cells exhibited enhanced UV sensitivity under quiescent conditions compared with asynchronously growing conditions. Finally, we show that the NER-dependent H2AX phosphorylation is also observed in murine peripheral T lymphocytes, typical nonproliferating quiescent cells *in vivo*. These results suggest that *in vivo* quiescent cells may suffer from NER-mediated secondary DNA damage including ssDNA and DSB.

To respond to numerous genotoxic stresses, cells have developed sophisticated signal transduction pathways that are collectively known as DNA damage response (DDR)[4] (1–3). The DDR senses DNA damage and activates various cellular mechanisms such as DNA repair, cell cycle checkpoint, and apoptosis. It has been becoming clear that a wide variety of covalent histone modifications are involved in DDR (4, 5). One of the best characterized examples is the phosphorylation of histone H2AX, a variant form of the core histone H2A (6). The H2AX has a conserved SQ motif known to be a target for the phosphoinositide 3-kinase-related protein kinases. In humans, the serine 139 residue within this motif is rapidly phosphorylated in response to DNA double-strand breaks (DSB), which is mainly mediated by ATM (ataxia-telangiectasia mutated), although DNA-PK (DNA-dependent protein kinase) redundantly functions. The phosphorylated H2AX (γH2AX) plays a pivotal role in recruiting various DDR factors such as MDC1 around DSB sites and amplifying the DDR signaling.

Although UV light from germicidal lamps (254 nm) dominantly produces cyclobutane pyrimidine dimers (CPDs) and 6-4 photoproducts (6-4PP) but not DSB directly (7), UV exposure also induces H2AX phosphorylation triggered by single-stranded DNA (ssDNA) regions formed by at least two different mechanisms. One is S phase-dependent and is initiated by replication arrest (8–10). The second type of UV-induced H2AX phosphorylation is observed outside the S phase and depends on nucleotide excision repair (NER) (11–14). The NER-dependent H2AX phosphorylation is much more profound in quiescent G_0 phase compared with cycling G_1 phase cells (14). Recently, it has been also reported that ssDNA breaks by Ape1 endonuclease might initiate H2AX phosphorylation in non-cycling cells exposed to UV (15). In all cases, UV-induced H2AX phosphorylation is triggered by secondary DNA lesions (*i.e.* ssDNA regions) and mediated by ATR (ATM- and Rad3-related), but not ATM.

The NER-mediated secondary DNA damage formation in quiescent cells would be a serious problem specifically *in vivo*,

* This work was supported by Grants 21510055 and 24510068 from the Ministry of Education, Culture, Sports, Science and Technology of Japan and also grants from Hokkoku Cancer Foundation (to T. M.) and Takeda Science Foundation (to M. W.).

[1] Both authors contributed equally to this work.

[2] Present address: Div. of Genetics and Mutagenesis, National Institute of Health Sciences, Tokyo 158-8501, Japan.

[3] To whom correspondence should be addressed: Faculty of Pharmacy, Institute of Medical, Pharmaceutical and Health Sciences, Kanazawa University, Kakuma-machi, Kanazawa 920-1192, Japan, Tel.: 81-76-234-4487; Fax: 81-76-234-4427; E-mail: matsukas@p.kanazawa-u.ac.jp.

[4] The abbreviations used are: DDR, DNA damage response; NER, nucleotide excision repair; DSB, DNA double-strand break; ssDNA, single-stranded DNA; CPD, cyclobutane pyrimidine dimer; 6-4PP, 6-4photoproducts; Ape1, apurinic/apyrimidinic endonuclease 1; XP, xeroderma pigmentosum; Ara-C, cytosine-β-D-arabinofuranoside.

because the majority of *in vivo* cells are known to be quiescent or quiescent-like. The NER is a universal and versatile repair mechanism for removing various helix-distorting DNA lesions such as UV-induced CPD and 6-4PP, as well as chemical-induced bulky base adducts (16). The NER reaction consists of multiple steps including lesion recognition, local unwinding around a lesion, dual incisions, removal of a lesion-containing oligonucleotide (~30 nucleotides), gap-filling DNA synthesis, and ligation to parental DNA (17), which require more than 30 polypeptides in an *in vitro* reconstitution (18). Defects in the preincision step of NER cause a genetically inherited cancer-prone disease, xeroderma pigmentosum (XP), characterized by a hypersensitivity to UV light and a high incidence of skin cancer in sun-exposed area (19). The NER-deficient XP patients are genetically classified into seven different complementation groups (XP-A through XP-G) depending on which NER gene contains causal mutation. Under quiescent conditions, primary fibroblasts derived from XP-A, XP-C, and XP-G patients exhibited no H2AX phosphorylation after UV exposure (14), clearly indicating its dependence on NER reaction rather than one particular NER factor. Based on the recruitment of RPA (replication protein A) and ATRIP (ATR interacting protein) to locally damaged sites, as well as the strong enhancement of NER-dependent H2AX phosphorylation by cytosine-β-D-arabinofuranoside (Ara-C) treatment, we proposed a model in which persistent ssDNA gaps caused by uncoupling of dual incision and gap-filling DNA synthesis might induce ATR-mediated H2AX phosphorylation. Correspondingly, quiescent cells exhibited low levels of DNA polymerase δ and ϵ catalytic subunits and PCNA (proliferating cell nuclear antigen) involved in the gap-filling reaction.

In this study, we have characterized the NER-dependent secondary DNA damage initiating H2AX phosphorylation in quiescent cells in more detail and tested the possibility of its formation in quiescent cells *in vivo*. We show that, in addition to ssDNA gaps, DSB is generated in an NER-dependent manner following UV, leading to the activation of ATM signaling pathways. Importantly, the activated ATM signaling partly contributes to UV resistance in human quiescent cells. We further show that UV-irradiated peripheral T lymphocytes cause NER-dependent H2AX phosphorylation, suggesting the applicability of our model to quiescent cells *in vivo*.

EXPERIMENTAL PROCEDURES

Cell Culture and UV Irradiation—Human primary fibroblasts, TIG-120 (Normal), XP2BI (XP-G) and AT2KY (A-T), and hTERT-transformed cell lines, SuSa/T-n (Normal), XP3OS/T-n (XP-A) and AT1OS/T-n (A-T), were obtained as described previously (14) and cultured in Dulbecco's modified Eagle's medium (Sigma) supplemented with 10% FBS and 50 μg/ml gentamicin in a 37 °C incubator at 5% CO_2. For G_0 synchronization, the cells were cultured in normal medium for 4 days to near confluency and subsequently in the medium containing 1% FBS for a further 3 or 4 days. Under the quiescent condition, labeling indexes were less than 1% in all cell strains used in this study. UV irradiation was performed with germicidal lamps (Toshiba, Tokyo, Japan) as described previously (14).

In a clonogenic survival assay, appropriate numbers of asynchronously growing or G_0-arrested SuSa/T-n and AT1OS/T-n cells were plated into 60-mm dishes in triplicate per each sample and incubated for 6 h to attach to the dishes. After washing with PBS(−) twice, the cells were irradiated with various doses of UV and incubated for 2–3 weeks. The colonies formed were fixed with ethanol, stained with 5% Giemsa solution, and counted under a stereomicroscope (Olympus, Tokyo, Japan).

Antibodies and Chemicals—Specific antibodies used in this study were anti-MRE11 (Gene Tex, Irvine, CA), anti-NBS1 (Oncogene Science, Cambridge, MA), anti-MDC1 (Bethyl Laboratories, Montgomery, TX), anti-phospho-H2AX (Ser^{139}; Cell Signaling, Danvers, MA; Upstate, Temecula, CA), anti-phospho-ATM (Ser^{1981}; Epitomics, Burlingame, CA), anti-phospho-Chk2 (Thr^{168}; Cell Signaling), anti-ssDNA (Immuno-Biological Laboratories, Gunma, Japan), anti-polymerase δ 125-kDa CS and anti-polymerase ϵ 258-kDa CS (BD Biosciences, San Jose, CA), anti-PCNA (Merck), and anti-β-actin (Bio Vision, Milpitas, CA). Anti-53BP1 antibody was kindly provided by Dr. Kuniyoshi Iwabuchi (Kanazawa Medical University, Kanazawa, Japan). The PI3K inhibitor LY294002 was purchased from Sigma. The ATM inhibitor KU-55933 and the DNA-PK inhibitor NU7026 were obtained from Abcam (Cambridge, UK). These inhibitors were dissolved in DMSO and used at the indicated concentration.

Immunofluorescence Staining—Immunofluorescence staining was performed essentially as described previously (14). Cells were fixed either in methanol/acetone (1:1) at −20 °C for 10 min or 4% formaldehyde at room temperature for 15 min. In the latter case, the fixed cells were further permeabilized with 0.5% Triton X-100 in 10 mM PBS (pH 7.4) at room temperature for 5 min. For ssDNA staining, cells were treated with 10 mM PBS (pH 7.4) containing 0.2% Triton X-100 on ice before fixation. After blocking with 20% FBS in 10 mM PBS (pH 7.4), cells were treated with appropriate primary antibody and subsequently Alexa Fluor™ 488 goat anti-mouse IgG (H+L) conjugate or Alexa Fluor™ 488 goat anti-rabbit IgG (H+L) conjugate (Molecular Probes, Eugene, OR). For the co-detection of UV-induced DNA damage, the stained cells were refixed with 2% formaldehyde and treated with 2 M HCl to denature their DNA. The cells were sequentially labeled either with anti-CPD monoclonal antibody (TDM-2) (20) and Alexa Fluor 594 goat anti-mouse IgG2a conjugate (Molecular Probes) or with anti-6-4PP monoclonal antibody (64M-5) (20) and Alexa Fluor 594 goat anti-mouse IgG conjugate (Molecular Probes). DAPI (Molecular Probes) was used for nuclear counterstaining. Fluorescence images were obtained with an all-in-one fluorescence microscope BZ-9000 (Keyence, Osaka, Japan) or confocal laser scanning microscope LSM710 (Carl Zeiss, Jena, Germany).

Western Blotting—Cells were lysed in Nonidet P-40 lysis buffer (50 mM Tris-HCl, pH 7.5, 150 mM NaCl, 1% Nonidet P-40) supplemented with protease inhibitor mixture (Roche Applied Science) and phosphatase inhibitor cocktails 1 and 2 (Sigma) or SDS sample buffer (125 mM Tris, 4% SDS, 20% glycerol, 0.01% bromphenol blue, 10% β-mercaptoethanol). Cell lysates were subjected to SDS-polyacrylamide gel electrophoresis and blotted onto Immobilon-P membrane (Merck). After blocking with 0.5% skim milk in PBS-T (10 mM PBS, pH 7.4,

0.05% Tween 20), the membranes were incubated with specific antibodies listed above and subsequently with horseradish peroxidase-conjugated anti-mouse or anti-rabbit IgG (Thermo Fisher, Rockford, IL). Following a chemiluminescence reaction with the Immobilon western chemiluminescent HRP substrate (Merck Millipore), protein bands were visualized using a LAS4000 lumino-image analyzer and quantified with Multi Gauge software version 3.0 (GE Healthcare, Pittsburgh, PA) or Image Studio Analysis software version 4.0 (LI-COR, Lincoln, NE).

DSB Detection—DSB formation was analyzed by the neutral comet assay according to the manufacturer's protocol (Comet assay kit; Trevigen, Gaithersburg, MD). After UV irradiation, SuSa/T-n or XP3OS/T-n cells were trypsinized and resuspended in PBS(−) at 2×10^5/ml. Cells were mixed with molten agarose and transferred onto glass slides. The slides were immersed in prechilled lysis solution for 30 min, followed by equilibration in 1× Tris borate-EDTA (TBE) buffer for 15 min. The samples were electrophoresed at 20 V for 20 min in 1× TBE and stained with SYBR Green I. Images were obtained with an all-in-one fluorescence microscope BZ-9000, and tail moment was measured in at least 100 cells using a CometScore™ program (TriTek Corp., Sumerduck, VA).

Isolation of T Lymphocytes and Flow Cytometric Analysis—Thymus and lymph nodes were isolated from wild-type or xpa knock-out C57BL/6 mice. The animal experiments were approved by the animal care and use committee of Kanazawa University and conducted in compliance with its guidelines. T lymphocytes were purified by removing B cells using Dynabeads M-450 sheep anti-mouse IgG (H+L) (Dynal Biotech, Oslo, Norway). The isolated T lymphocytes were irradiated with UV or treated with etoposide (Sigma) and cultured in RPMI 1640 medium supplemented with 10% heat-inactivated FBS and 50 μg/ml gentamicin in a 37 °C incubator at 5% CO_2. Flow cytometric analyses of H2AX phosphorylation were performed with anti-γH2AX antibody as described previously (14).

RESULTS

Activation of ATM Signaling in Quiescent Human Cells following UV Irradiation—In the previous study, we observed NER-dependent accumulation of 53BP1 in locally UV-irradiated subnuclear regions of quiescent cells (14). 53BP1 is one of the DDR factors involved in DSB signaling and co-localizes with γH2AX foci following ionizing radiation (21). In this study, we have first tested whether other DSB signaling factors accumulate after local UV irradiation. Human primary fibroblasts (TIG-120) were arrested in the G_0 phase by a combination of contact inhibition and serum starvation and locally irradiated with UV through an isopore membrane filter. The immunofluorescence staining with specific antibodies revealed the accumulation of MRE11 (meiotic recombination 11), NBS1 (Nijmegen breakage syndrome 1), and MDC1 (mediator of DNA damage checkpoint protein 1) 1 h post-UV (Fig. 1*A*). In clear contrast, NER-deficient XP2BI (XP-G) cells failed to exhibit the local accumulation of those DDR factors, suggesting that these responses are mediated by NER, but not directly by UV.

We next asked whether ATM kinase is activated following UV irradiation under quiescent conditions. G_0-arrested TIG-120 cells were irradiated with UV, and their lysates were recovered after 1–4 h of incubation. Western blot analysis with phospho-specific antibodies revealed that ATM Ser^{1981} and Chk2 Thr^{68} are phosphorylated at 1 h following UV, whereas γH2AX formation was gradually increased up to 4 h (Fig. 1*B*). Again, the phosphorylation of ATM and Chk2 was not observed in NER-deficient XP2BI cells (Fig. 1*B*). To confirm the NER dependence of the phosphorylation reaction, we performed a dose-response type of experiment using other NER-deficient cell line, XP3OS/T-n, which was derived from an XP-A patient and immortalized by hTERT introduction (22). An NER-proficient control cell line, SuSa/T-n, exhibited UV dose-dependent increase of ATM and Chk2 phosphorylation ranging 10–40 J/m^2, whereas NER-deficient XP3OS/T-n cells showed only marginal phosphorylation (Fig. 1*C*). In addition, ectopic expression of Myc-tagged XPA complemented the inability of UV-irradiated XP3OS/T-n cells to repair 6-4PP as well as to induce the phosphorylation of ATM and Chk2 (Fig. 1*D*). These results clearly indicate that in quiescent cells, ATM signaling is activated within 1 h after UV in an NER-dependent manner.

We further analyzed whether the NER-dependent accumulation of DDR factors depends on ATM activation. AT2KY cells from an A-T patient were arrested in G_0 phase by contact inhibition/serum starvation and pretreated with a PI3K inhibitor LY294002 to inhibit DNA-PK activity, because DNA-PK functions redundantly in the absence of ATM (23). AT2KY cells have no full-length ATM (24) and showed no signals of phosphorylated ATM at Ser^{1981} following ionizing radiation, whereas their NER activity is completely normal.[5] Under ATM- and DNA-PK-defective conditions, we failed to observe the local accumulation of MRE11, NBS1, and 53BP1 after micropore UV irradiation (Fig. 2*A*), suggesting that the recruitment of DDR factors depends on ATM and/or DNA-PK activity. To examine their implication separately, we decided to employ specific inhibitors for ATM (KU-55933) and DNA-PK (NU7026). As expected, the treatment with KU-55933, but not NU7026, fully suppressed UV-induced phosphorylation of ATM and Chk2 (Fig. 2*B*). We evaluated the impacts of the two inhibitors on MRE11 accumulation in UV-irradiated subnuclear regions, which were monitored with anti-CPD antibody. As shown in Fig. 2*C*, KU-55933, but not NU7026, significantly impaired the local accumulation of MRE11, suggesting that ATM kinase plays a dominant role in the efficient recruitment of DDR factors.

NER-dependent DSB Formation in Quiescent Human Cells following UV Irradiation—Having observed the activation of ATM kinase, as well as ATM-dependent recruitment of DDR factors, we next tried to detect DSB in UV-irradiated quiescent cells using the comet assay. The NER-proficient human cell line SuSa/T-n was arrested in G_0 phase and irradiated with 10–40 J/m^2 of UV. After 1-h incubation, the cells were subjected to the neutral comet assay, and tail moment was measured as described under "Experimental Procedures." As shown in Fig. 3

[5] T. Sasaki and T. Matsunaga, unpublished data.

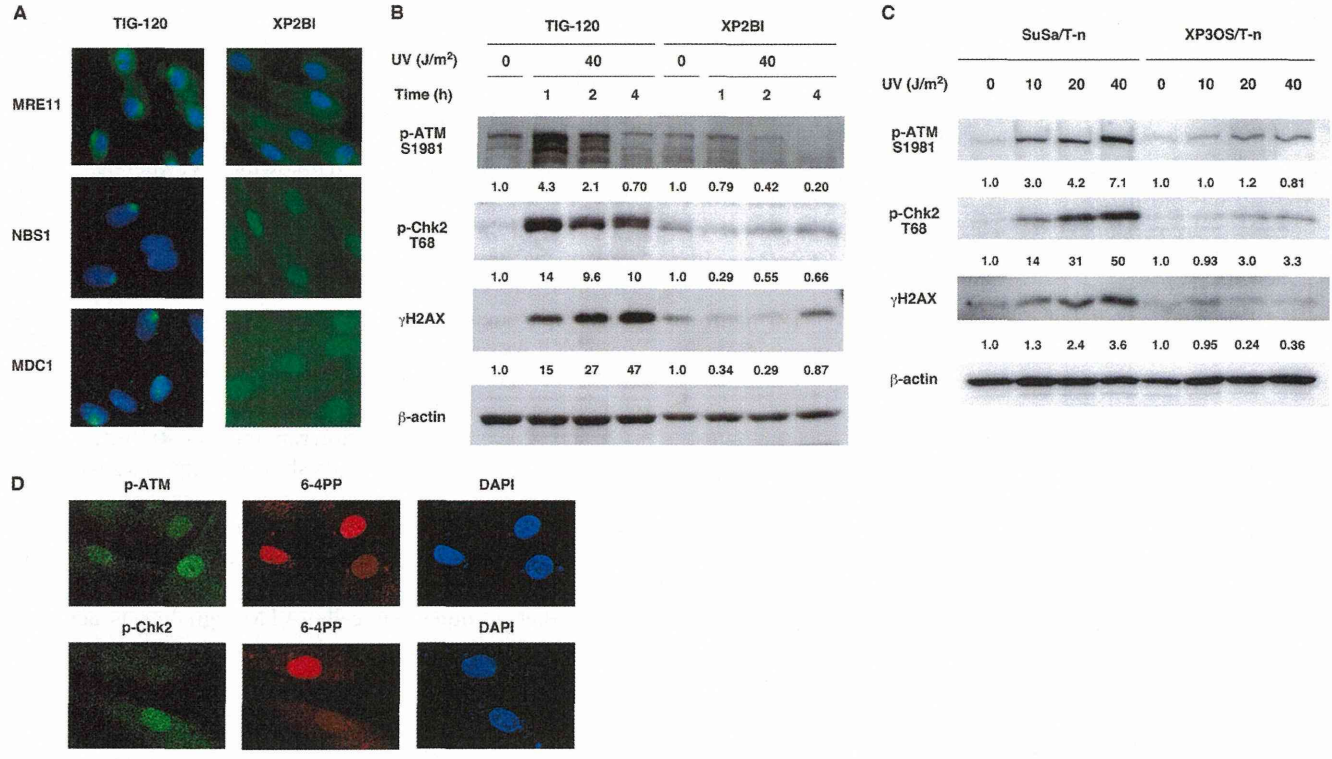

FIGURE 1. **NER-dependent recruitment of DDR factors and ATM activation in quiescent human cells.** *A*, TIG-120 or XP2BI cells were arrested in the G_0 phase by contact inhibition/serum starvation and locally irradiated with 40 J/m^2 of UV through an isopore membrane filter (pore size, 8 μm). After 1-h incubation, cells were fixed and stained with the indicated antibodies and DAPI. *B*, G_0-arrested TIG-120 or XP2BI cells were irradiated with 40 J/m^2 of UV and incubated for up to 4 h. Cell lysates were prepared and analyzed by Western blotting with the indicated antibodies. The relative signal intensities to unirradiated control were determined by Multi Gauge software and shown in the figure. *C*, G_0-arrested SuSa/T-n or XP3OS/T-n cells were irradiated with 10–40 J/m^2 of UV. After 1-h incubation, cell lysates were prepared and analyzed by Western blotting as described above. *D*, XP3OS/T-n cells were transfected with pCMV-Myc-XPA plasmid using FuGENE HD transfection reagent (Promega) and arrested in the G_0 phase by contact inhibition/serum starvation. At 2 h post-UV irradiation (40 J/m^2), the cells were fixed and double-stained with anti-6-4PP and anti-pATM (Ser^{1981}) or anti-pChk2 (Thr^{168}) antibodies.

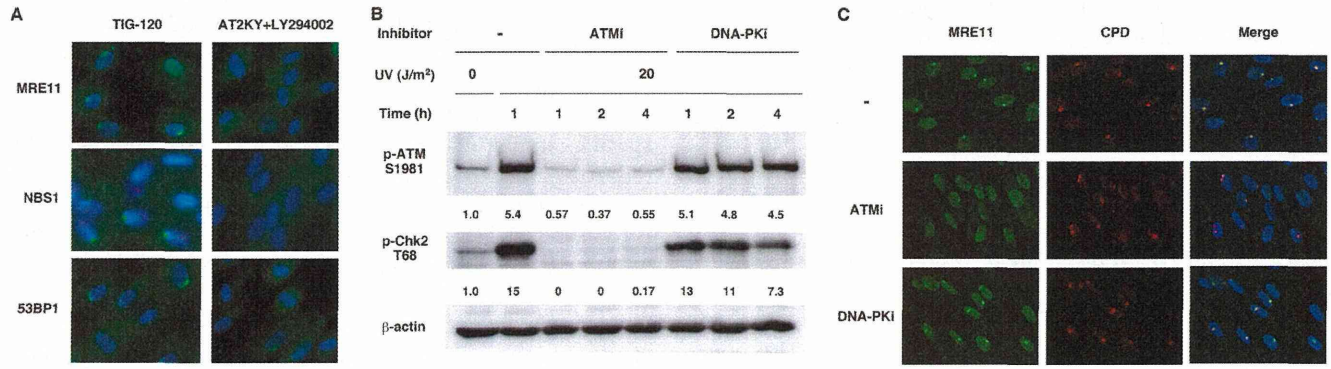

FIGURE 2. **The NER-dependent recruitment of DDR factors mainly depends on ATM activity.** *A*, TIG-120 or AT2KY cells were arrested in G_0 phase and locally irradiated with 40 J/m^2 of UV through an isopore membrane filter (pore size, 8 μm). After 1-h incubation, the cells were fixed and immunostained with the indicated antibodies. Note that AT2KY cells were treated with 100 μM LY294002 for 30 min before UV irradiation and during post-UV 1-h incubation. *B*, G_0-arrested TIG-120 cells were pretreated with or without either 10 μM KU-55933 (ATMi) or 10 μM NU7026 (DNA-PKi) for 30 min. The cells were irradiated with 20 J/m^2 of UV and incubated with or without each inhibitor for 1–4 h before cell lysis. The phosphorylation of ATM and Chk2 was analyzed by Western blotting with phospho-specific antibodies to Ser^{1981} and Thr^{68}, respectively. *C*, G_0-arrested TIG-120 cells were pretreated with ATMi or DNA-PKi as described above and locally irradiated with 40 J/m^2 of UV through an isopore membrane filter (pore size, 5 μm). After 1-h incubation with each inhibitor, the cells were co-immunostained with anti-MRE11 and anti-CPD antibodies.

(*A* and *B*), SuSa/T-n cells exhibited elongated comet tails following UV and a dose-dependent increase of tail moment. In clear contrast, NER-deficient XP3OS/T-n (XP-A) cells failed to show the elongation of comet tails (Fig. 3, *B* and *C*). These results strongly suggest that DSB is indeed generated in UV-irradiated quiescent cells in an NER-dependent manner.

ATM Partly Contributes to UV-induced H2AX Phosphorylation as Well as UV Resistance in Quiescent Human Cells—The findings of NER-dependent DSB formation and ATM activation 1 h post-UV in quiescent cells prompted us to test whether the early fraction of UV-induced H2AX phosphorylation is mediated by ATM. G_0-arrested TIG-120 cells were pretreated